physica status solidi rrl
www.pss-rapid.com

Element-Specific Magnetization Damping in Ferrimagnetic $DyCo_5$ Alloys Revealed by Ultrafast X-ray Measurements

*Radu Abrudan, Martin Hennecke, Florin Radu, Torsten Kachel, Karsten Holldack, Rolf Mitzner, Andreas Donges, Sergii Khmelevskyi, András Deák, László Szunyogh, Ulrich Nowak, Stefan Eisebitt, and Ilie Radu**

The dynamic response of magnetically ordered materials to an ultrashort external stimulus depends on microscopic parameters, such as magnetic moment, exchange, and spin–orbit interactions. Whereas it is well established that, in multicomponent magnetic alloys and compounds, the speed of demagnetization and spin switching processes has an element-specific character, the magnetization damping was assumed to be a universal parameter for all constituent magnetic elements irrespective of their different spin–orbit couplings and electronic structure. Herein, experimental and theoretical evidence for an element-specific magnetic damping parameter is provided by investigating the ultrafast magnetization response of a high-anisotropy ferrimagnetic $DyCo_5$ alloy to femtosecond laser excitation. Strikingly different demagnetization and remagnetization dynamics of Dy and Co magnetic moments is revealed by employing femtosecond laser pump–X-ray magnetic circular dichroism probe measurements combined with atomistic spin dynamics (ASD) simulations using ab initio calculated parameters. These observations, fully corroborated by the ASD simulations, are linked to the element-specific spin–orbit coupling strengths of Dy and Co, which are incorporated in the phenomenological magnetization damping parameters. These findings can be used as a recipe for tuning the speed and magnitude of laser-driven magnetic processes and consequently allow control over various dynamic functionalities in multicomponent magnetic materials.

1. Introduction

Manipulation and control of magnetism by light is one of the key concepts of modern research in magnetism with direct and far-reaching implications for magnetic data recording.[1,2] Of particular interest for both fundamental and applied science is the use of femtosecond (fs) laser pulses to fully control the orientation of a spin ensemble on ultrashort timescales. A cornerstone in this respect was the discovery of thermally induced magnetization switching in ferrimagnetic GdFeCo via a single fs laser pulse excitation. This ultrafast spin switching process was mediated by an unexpected transient ferromagnetic-like state (TFLS), which has been identified as the driving microscopic mechanism behind thermally induced switching in ferrimagnetic alloys.[3]

The existence of the TFLS is related to the different demagnetization rates of the transition metal (TM) and rare-earth (RE) constituents in the alloy.[3,4] This is commonly linked to the larger magnetic moment of the RE spins, e.g., $\mu_{Gd} = 7.63\,\mu_B$

Dr. R. Abrudan, Dr. F. Radu, Dr. T. Kachel, Dr. K. Holldack, Dr. R. Mitzner
Helmholtz-Zentrum Berlin für Materialien und Energie
BESSY II
Albert-Einstein-Str. 15, Berlin 12489, Germany

Dr. M. Hennecke, Prof. S. Eisebitt, Dr. I. Radu
Max Born Institute for Nonlinear Optics and Short Pulse Spectroscopy
Max-Born-Strasse 2A, Berlin 12489, Germany
E-mail: radu@mbi-berlin.de

Dr. A. Donges, Prof. U. Nowak
Fachbereich Physik
Universität Konstanz
Universitätsstraß e 10, Konstanz 78457, Germany

The ORCID identification number(s) for the author(s) of this article can be found under https://doi.org/10.1002/pssr.202100047.

DOI: 10.1002/pssr.202100047

Dr. S. Khmelevskyi
Research Center for Computational Materials Science and Engineering
Vienna University of Technology
Karlsplatz 13, Vienna A-1040, Austria

Dr. A. Deák, Prof. L. Szunyogh
Department of Theoretical Physics
Budapest University of Technology and Economics
Budafoki út 8, Budapest H-1111, Hungary

Dr. A. Deák, Prof. L. Szunyogh
MTA-BME Condensed Matter Research Group
Budapest University of Technology and Economics
Budafoki út 8, Budapest H-1111, Hungary

Prof. S. Eisebitt
Institut für Optik und Atomare Physik
Technische Universität Berlin
Straße des 17. Juni 135, Berlin 10623, Germany

Dr. I. Radu
Fachbereich Physik
Freie Universität Berlin
Arnimallee 14, Berlin 14195, Germany

compared with $\mu_{Fe} = 1.92\,\mu_B$,[4] leading to slower spin dynamics with respect to the TM spins. However, the demagnetization times τ_i[5]

$$\tau_i \approx \frac{\mu_i}{2\alpha_i\gamma_i k_B T} \tag{1}$$

do not only depend on the magnetic moments μ_i but also on the spin–orbit coupling strength of the respective elements, which, in atomistic spin models, is contained in the damping parameter α_i;[6–8] γ_i denotes the gyromagnetic ratio, k_B is the Boltzmann constant, and T denotes the temperature of either the electronic or phononic subsystems—see also Equation (4) and (5). Previous studies on ultrafast switching often assumed that the damping parameter α_i is universal for all spins in the compound, and despite this approximation, these models provided reasonable agreement with experimental observations so far.[3,4,9,10] Yet, as we will show in the following, a quantitative understanding of ultrafast spin dynamics in complex multi-sublattice ferrimagnets requires a more detailed knowledge of the damping mechanisms on an atomistic level.

In this work, we present an element- and time-resolved study of ferrimagnetic $DyCo_5$ alloy with a focus on the demagnetization processes of the constituent Dy and Co elements. The choice of $DyCo_5$ alloy has been motivated by the existence of large and different elemental spin–orbit coupling strengths and magnetic moments at Dy and Co sites, with the former being expected to presumably generate different magnetic damping behaviors of the constituent elements. The experimental observations reveal distinctly different demagnetization times and remagnetization behaviors for Dy and Co. To understand the time evolution of these processes, we use atomistic spin dynamics (ASD) simulations using an ab initio calculated spin Hamiltonian.[11] Simulation results and the X-ray magnetic circular dichroism (XMCD) measurements are compared in a quantitative manner to determine the distinct, element-specific damping coefficients of Dy and Co spins. The experimental XMCD data can only be described using largely different elemental magnetic damping constants for Co and Dy. These findings provide the first direct experimental and theoretical evidence for an element-specific damping in ferrimagnetic alloys.

2. Results and Discussion

2.1. Ferrimagnetic $DyCo_5$ and Time-Resolved XMCD Method

The $DyCo_5$ sample is an intermetallic stoichiometric phase of $Dy_{1-x}Co_x$ alloys and a highly anisotropic magnetic system with remarkably strong magnetocrystalline anisotropies per sublattice, which are, e.g., comparable with the Dy–Co intra- and interatomic exchange interaction energies (see the previous study[11] and the following). Dy and Co sublattices are aligned in a ferrimagnetic structure, as sketched in **Figure 1**b. $DyCo_5$ exhibits both, a magnetization compensation and a spin-reorientation transition, and it has attracted increased attention recently as a prototype ferrimagnetic alloy.[11–15] Polycrystalline $DyCo_5$ films of 25 nm thickness with perpendicular magnetic anisotropy were grown by magnetron sputtering in an ultraclean argon atmosphere at room temperature. The stoichiometry of the ferrimagnetic alloy was controlled by varying the deposition rate of separate chemical elements during cosputtering. Aluminum membranes (500 nm thick) have been used as substrates due to their large transmission in the soft X-ray spectral range and to ensure maximum stability during laser pumping experiments. Detailed sample characterization was performed prior to the pump–probe experiments using the ALICE diffractometer[16] at BESSY II synchrotron and has been reported elsewhere.[11]

To measure the element-specific magnetization dynamics at Dy and Co absorption edges in $DyCo_5$, we used time-resolved XMCD at the fs-slicing facility of the BESSY II electron storage ring, which provides 100 fs soft X-ray pulses with circular polarization.[17] XMCD measurements were performed in transmission geometry (Figure 1a), recording the intensity of the transmitted X-ray beam with an avalanche photodiode (APD) upon flipping the external magnetic field direction (±250 mT). Stroboscopic laser pump/X-ray probe measurements were performed using 40 fs (full width at half maximum) laser pulses of 1.5 eV photon energy; the subsequent laser-induced magnetization dynamics was measured by recording the XMCD signal using 100 fs X-ray pulses tuned to the L_3 edge of the Co (778 eV) and the M_5 edge of Dy (1295 eV). Element selectivity, provided by the X-ray transitions involving core electrons, allows us to probe separately the dynamics of the 3d and 4f magnetic moments of Co and Dy, respectively. Measurements were performed at two different incident laser fluences of 9.4 and 14.1 mJ cm^2. The sample temperature was kept at 150 K during the pump–probe measurements, i.e., above the compensation temperature $T_{comp} = 125$ K and below the spin-reorientation transition region $T_{SR1,2} = 320$–360 K.[11]

2.2. ASD Simulations

Figure 1b shows the crystallographic $CaCu_5$-type structure of the $DyCo_5$ alloy with the Dy and Co spins being antiferromagnetically coupled and parallel with the ab basal plane of the unit cell; this spin configuration is retained up to the spin-reorientation temperature $T_{SR1,2} = 320$–360 K. To model the ultrafast demagnetization of $DyCo_5$, we use our previously developed multiscale model of ab initio calculations and ASD simulations (see the previous study[11]). Self-consistent field calculations were performed in terms of the scalar-relativistic Korringa–Kohn–Rostoker (KKR) method within the atomic sphere approximation[18,19] and the local spin-density approximation (LSDA), where the nine 4f electrons of Dy were treated within the frozen-core approximation. The isotropic exchange couplings were then calculated in the spirit of the magnetic force theorem.[20] The magnetic anisotropy energies were obtained from the relativistic local density approximation (LDA) $+U$ method used within the KKR formalism[21,22] in terms of the magnetic force theorem as a difference of the band energies corresponding to different spin quantization axes.

The spin Hamiltonian for the normalized magnetic moments $\mathbf{S}_i = \boldsymbol{\mu}_i/\mu_i$ reads

$$\mathcal{H} = -\sum_{i,j} J_{ij}\mathbf{S}_i \cdot \mathbf{S}_j - \mathbf{B} \cdot \sum_i \mu_i \mathbf{S}_i + \sum_i d^z_{2,i}\sin^2\vartheta_i + \sum_i d^6_{6,i}\sin^6\vartheta_i \cos(6\varphi_i) \tag{2}$$

accounting for the exchange interaction, Zeeman interaction with an external magnetic field, and the elemental magnetic

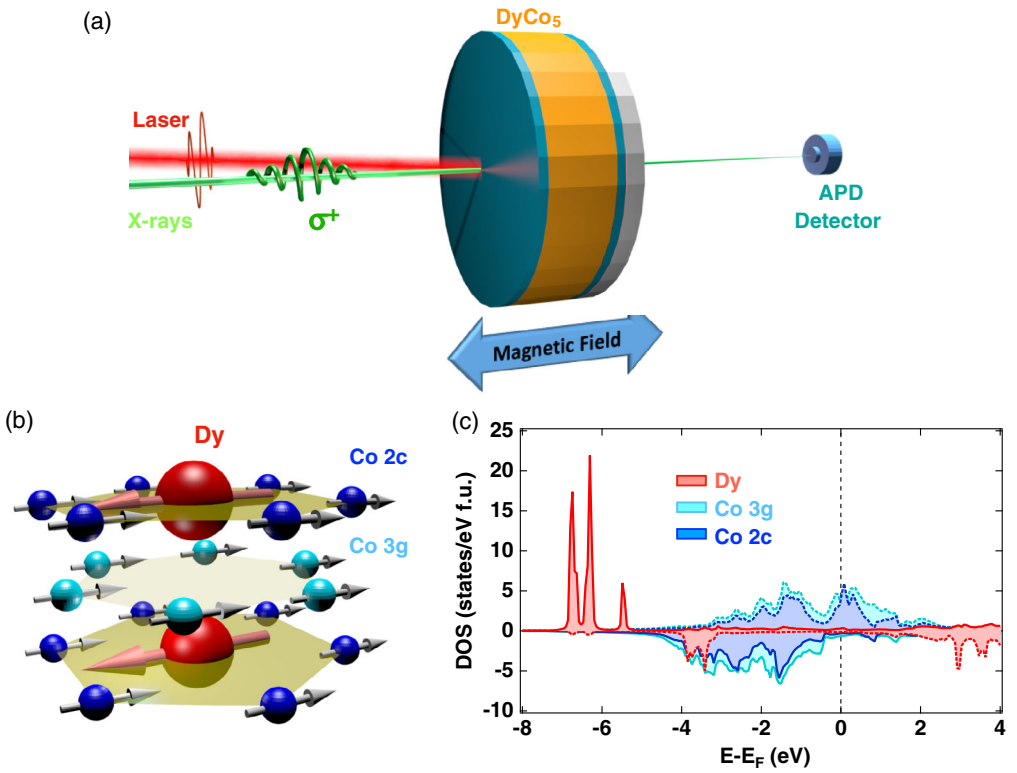

Figure 1. a) Schematic illustration of the time-resolved XMCD measurement geometry. The fs X-rays and laser pulses are collinearly impinging on $DyCo_5$ sample in a transmission pump–probe geometry; thin Ta films (blue sheets) are used as buffer and capping layers. The transmitted X-ray intensity is measured using an APD detector. b) Representation of the ferrimagnetic spin structure of $DyCo_5$ for an out-of-plane magnetization configuration, as used in the XMCD experiments; the basal plane of the hcp unit cell is perpendicular to the $DyCo_5$ sample surface. c) Element- and spin-resolved density of states (DOS) for $DyCo_5$ alloy obtained from ab initio calculations showing the antiferromagnetic coupling of Dy and Co. The spin-up and spin-down DOS states are depicted by solid and dashed lines, respectively.

anisotropies, respectively; J_{ij} are the Heisenberg exchange interactions, $d^z_{2,\mathrm{Dy}} = -1.4$ mRy and $d^z_{2,\mathrm{Co}} = +0.1$ mRy are the competing uniaxial anisotropy energies of Dy and Co spins, respectively, $d^6_{6,\mathrm{Dy}} = 0.17$ mRy is a basal-plane anisotropy, and ϑ_i, φ_i are the polar coordinates of spin $\mathbf{S}_i$. As the laser excitation will heat the sample beyond the spin reorientation temperature, the long delay times simulations, shown in **Figure 2**c, require an external field $B = 15$ T to keep the magnetization aligned along the b-axis (i.e., the film normal). This magnetic field is larger than experimentally required fields to magnetically saturate the sample but much smaller than the effective exchange fields acting in the magnetically ordered state on the sublattice (calculated $J_{\mathrm{Co-Co}} = 1.1$ mRy and $J_{\mathrm{Dy-Co}} = -0.23$ mRy, see the previous study,[11] correspond to effective exchange fields of about 100 T for Dy and 1000 T for Co) and, thus, is not affecting the ultrafast demagnetization behavior. Moreover, ASD simulations with a reduced magnetic field of 100 mT instead of 15 T show a similar transient demagnetization behavior—see Supporting Information.

Using the spin Hamiltonian defined in Equation (2), we integrate the stochastic Landau–Lifshitz–Gilbert (LLG) equation of motion[23]

$$\frac{\partial \mathbf{S}_i}{\partial t} = \frac{-\gamma_i}{(1+\alpha_i^2)\mu_i}\mathbf{S}_i \times (\mathbf{H}_i + \alpha_i \mathbf{S}_i \times \mathbf{H}_i) \tag{3}$$

where $\gamma_i = g_i \mu_\mathrm{B}/\hbar$ is the gyromagnetic ratio (with $g_{\mathrm{Dy}} = 4/3$ and $g_{\mathrm{Co}} = 2$), and $\alpha_i = \alpha_i^{\mathrm{el}} + \alpha_i^{\mathrm{ph}}$ is the atomistic Gilbert damping coefficient. The effective field is

$$\mathbf{H}_i = -\frac{\partial \mathcal{H}}{\partial \mathbf{S}_i} + \boldsymbol{\zeta}_i^{\mathrm{el}} + \boldsymbol{\zeta}_i^{\mathrm{ph}} \tag{4}$$

with $\boldsymbol{\zeta}_i^{\nu}$ being Gaussian white noise with

$$\langle \boldsymbol{\zeta}_i^{\nu} \rangle = 0, \langle \boldsymbol{\zeta}_i^{\lambda}(0) \boldsymbol{\zeta}_j^{\nu}(t)^{\dagger} \rangle = \frac{2\alpha_i^{\nu} k_\mathrm{B} T_\nu \mu_i}{\gamma_i} \delta(t) \delta_{ij} \delta_{\nu\lambda} \tag{5}$$

The separation of the thermal noise $\boldsymbol{\zeta}_i^{\nu}$ and damping α_i^{ν} into the electronic and lattice contributions, denoted by index $\nu = \mathrm{el}, \mathrm{ph}$, is rationalized by the different electronic structures of the TM and RE metals;[24] δ_{ij} and $\delta_{\nu\lambda}$ denote the Kronecker deltas, and $\delta(t)$ is the delta distribution function. It is worth noting that the atomistic Gilbert damping parameter α_i^{ν} determines the amount of energy and angular momentum dissipated per elemental spin (or sublattice magnetization) precessional cycle into the heat bath, which acts here as an external reservoir.

In general, for the delocalized 3d moments of the TM, the demagnetization is due to scattering with hot conduction electrons, and thus, it is sufficient to couple the Co spins only to the electronic temperature via $\alpha_{\mathrm{Co}}^{\mathrm{el}}$,[5] i.e., $\alpha_{\mathrm{Co}}^{\mathrm{ph}} = 0$. The 4f states

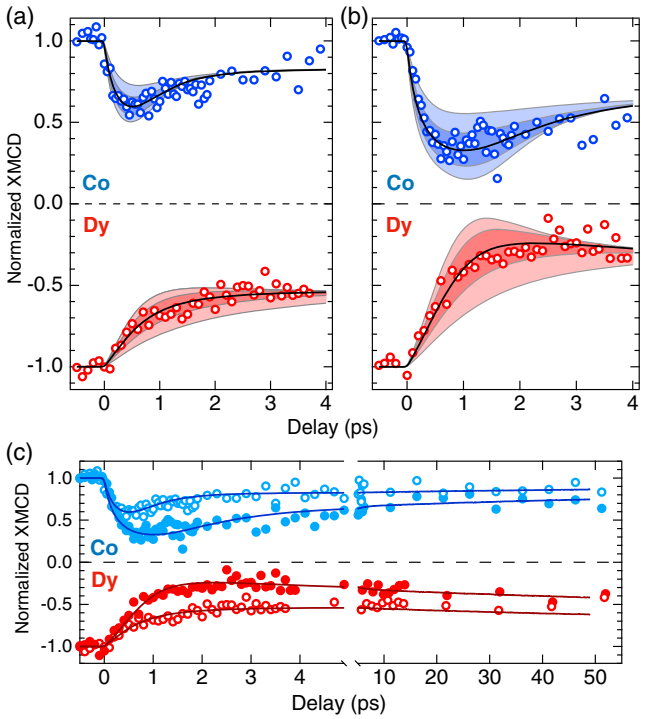

Figure 2. Time-resolved XMCD data showing the demagnetization behavior of Co (blue dots) and Dy (red dots). a,b) The data measured for the incident laser fluences of 9.4 and 14.1 mJ cm^{-2}, respectively. The ASD simulations performed for various magnetization damping parameters α_i are shown as continuous black and gray lines. The dark and light colored areas represent ±25% and ±50% variation of α_i from the optimum α_i values ($\alpha_{Co} = 0.004$ and $\alpha_{Dy} = 0.03$) describing the best match with the experimental data (black solid line). c) Long-time behavior of demagnetization and remagnetization dynamics measured for the two fluences shown in (a,b); the solid lines are the results of the corresponding ASD simulations.

of Dy are located well below Fermi level (Figure 1c); hence, there is only a weak coupling α_{Dy}^{el} to the electronic temperature stemming from the spin-polarized 5d6sp electrons, whereas the 4f moments only interact with the less excited lattice via α_{Dy}^{ph}.[4,24,25] However, due to the large 4f orbital moment of Dy, we expect that this 4f contribution to the Gilbert damping still plays a fundamental role in the demagnetization process; see, e.g., the previous studies.[24,26] Finally, we obtain the time-dependent electron and phonon temperatures T_ν in Equation (5) by solving the two-temperature model (2TM)—the details about the 2TM parameters can be found in the Supporting Information.

2.3. Element-Specific Magnetization Dynamics

The results of the laser-induced demagnetization of ferrimagnetic $DyCo_5$ measured element-specifically at the incident laser fluences of 9.4 and 14.1 mJ cm^{-2} (corresponding to demagnetization degrees of ≈ 40% and ≈ 80%, respectively) are shown in Figure 2. For both fluences, a clearly distinct demagnetization and remagnetization dynamics is visible for both Co and Dy sublattices. At Co sites, the demagnetization reaches its maximum in about 0.5 ps (depending on the laser fluence), whereas Dy needs 3–4 ps to achieve the same demagnetization amplitude. Such a disparity of the RE and TM demagnetization times has previously been observed in other RE-TM ferrimagnets.[3,27,28] Moreover, it is clear that in the temporal range where the Co magnetization has started to recover, Dy is not even fully demagnetized yet. For a better overview on the remagnetization processes, the transient XMCD data measured on longer pump–probe delays are shown in Figure 2c. We observe that around 50 ps time delay, Co is almost fully remagnetized, with about 80–90% of its initial XMCD values, whereas the Dy magnetization is still 40–60% demagnetized.

To retrieve the time constants of the demagnetization (τ_D) and remagnetization (τ_R) processes from the transient XMCD data, we use a biexponential fit function convolved with a Gaussian $g(t)$ accounting for the time resolution of the measurement of 110 fs

$$f(t) = g(t) \otimes \begin{cases} A, & t \leq 0 \\ A - B\exp\left(-\frac{t}{\tau_D}\right) - C\exp\left(-\frac{t}{\tau_R}\right), & t > 0 \end{cases} \quad (6)$$

where A describes the XMCD signal before the pump pulse arrival, whereas B and C are the amplitudes of the two exponentials describing the initial magnetization quenching and the subsequent relaxation processes, respectively. The retrieved time constants for the demagnetization and remagnetization processes of Co and Dy are listed in **Table 1**. The fitting curves of Dy and Co XMCD data are shown in the Supporting Information.

The elemental demagnetization times τ_D coincide for both applied fluences within our experimental error: Co demagnetizes within ≈ 200 fs, whereas for Dy, it takes about 1 ps. This is different for the respective remagnetization time τ_R, where we clearly observe a slowing down of the Co recovery with increasing fluence. Unfortunately, the relaxation time behavior at Dy sites is inconclusive due to large error bars, and therefore, an accurate comparison of Dy versus Co remagnetization times is difficult. We note, however, that the remagnetization time is more influenced by the values of the exchange integrals, which are responsible for the occurrence of the magnetic order, as well as by the maximum degree of spin disorder generated during the initial demagnetization process. Comparing our demagnetization times with recent measurements on amorphous CoDy alloys, we find, however, similar values for τ_D.[29]

Now, we turn to the comparison of the experimental and theoretical results. We obtain distinct, element-specific damping parameters of $\alpha_{Co}^{el} = 0.004$ and $\alpha_{Dy} = 0.03$ by minimizing the mean squared error between the combined Dy and Co XMCD data and the ASD simulation results, both displayed in Figure 2. Here, we assumed that the electronic contribution

Table 1. Demagnetization τ_D and remagnetization τ_R time constants of Co and Dy as determined by fitting the time-resolved XMCD data shown in Figure 2.

F [mJ cm^{-2}]	τ_D [fs]		τ_R [ps]	
	Dy	Co	Dy	Co
9.4	980 ± 120	175 ± 45	18.0 ± 9.3	1.85 ± 0.5
14.1	900 ± 160	210 ± 35	12.1 ± 6.7	4.20 ± 0.7

to the atomistic damping is similar for both elements and set $\alpha_{Dy}^{el} = \alpha_{Co}^{el} = 0.004$, thus leading to $\alpha_{Dy}^{ph} = 0.026$. This procedure gives us nearly identical values for both fluences, indicating the robustness of the theoretical model. In Figure 2a,b, the output of atomistic simulations is shown for variations of ±25% and ±50% of the α_i parameters for both elements and laser fluences. The best data match of the simulations is depicted by the thick black line, corresponding to $\alpha_{Co}^{el} = 0.004$ and $\alpha_{Dy} = 0.03$ damping parameters.

To further highlight the importance of an element-specific damping, we tried to reproduce the demagnetization data with the more common approach, namely, a single, universal damping constant α_{el} for both elements and with α_{Dy}^{ph} set to zero. The results are displayed in **Figure 3** with the dotted and dashed lines representing simulations for different values of $\alpha_{el} = 0.004$, 0.005, and 0.006. It becomes evident that a single damping constant does not reproduce simultaneously both the Dy and Co experimental data: while one could obtain a satisfactorily description of Co behavior using $\alpha_{el} = 0.004$, this is obviously not the case for Dy. Only upon introducing an extra damping term at Dy sites α_{Dy}^{ph}, and thus using an element-specific damping for Co and Dy, the ASD simulations can reproduce the experimental data with high accuracy (blue and red solid lines in Figure 3).

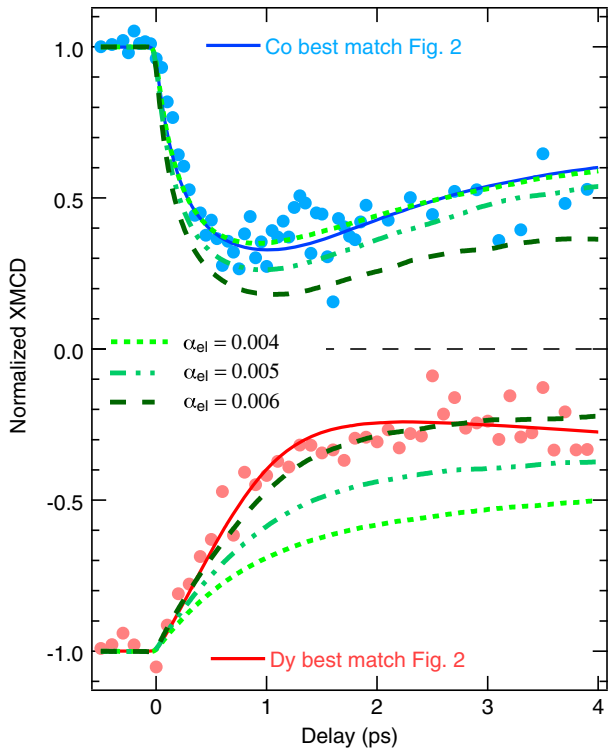

Figure 3. Comparison of the time-resolved XMCD measurements (solid dots) with the ASD simulations (green lines) performed using a single magnetic damping parameter α_{el} for both Dy and Co. Variation of the α_{el} values, as labeled in the figure, does not reproduce the transient XMCD data for both elements. The best match with the experimental data is obtained for clearly different magnetic damping parameters at Co and Dy sites, namely, $\alpha_{Co} = 0.004$ and $\alpha_{Dy} = 0.03$; the corresponding ASD simulation curves (blue and red solid lines) are taken from Figure 2.

The ASD simulations describe the experimental results only by choosing clearly different values of the magnetic damping parameters for each element, namely, $\alpha_{Co} = 0.004$ and $\alpha_{Dy} = \alpha_{el} + \alpha_{ph} = 0.03$. This is a surprising observation, because the ASD simulations are based on an ab initio-parametrized spin Hamiltonian with the elemental magnetic moment, magnetic anisotropy, and the exchange interaction being ab initio calculated; i.e., these are not variable parameters. The only free parameters in our spin model in Equation (2) and (3) are the magnetic damping parameters that can be adjusted to match the experimental data.

At this point, it is important to note the major differences between the atomistic Gilbert damping parameters used in our ASD simulations and a macroscopic damping parameter, as obtained, for instance, from ferromagnetic resonance measurements (FMR). Typically, an FMR-derived damping parameter contains both extrinsic (i.e., sample-specific damping due to spin scattering with defects, magnetic/structural inhomogeneities, two-magnon scattering, etc.) and intrinsic (e.g., due to electron–spin, lattice–spin interactions) contributions to magnetization relaxation and, hence, can be considered as an effective, macroscopic damping parameter. The atomistic Gilbert damping, on the other hand, accounts only for intrinsic spin relaxation effects at the microscopic level describing the local exchange of energy and angular momentum between the spins, the electronic system, and the crystal lattice.

To understand these observations, we first consider the microscopic origin of the damping parameters of Dy and Co spins in ferrimagnetic $DyCo_5$ in more detail, based on the different electronic structure of the RE and TM atoms.

The Co magnetic moment stems from 3d electrons that are hybridized with the delocalized 4sp electrons, which can be considered as a single magnetic moment coupled predominantly to the electronic thermal reservoir of the system. The spin-relaxation mechanism in such an itinerant, metallic 3*d* ferromagnet is dominated by ultrafast transversal spin excitation in the form of electron-magnon scattering,[5,30] quantified by α_{Co}^{el}. Additional longitudinal Stoner excitations and Elliott–Yaffet spin-flip scattering[31,32] are not considered in our extended Heisenberg formalism, but recent studies suggest that they play only a secondary role in ultrafast demagnetization.[30,33]

Dy atoms, on the other hand, exhibit highly localized 4f moments, which couple via intraatomic exchange to the itinerant 5d6sp electrons.[4,25] As such, their magnetization damping can be described by an s–f model,[34] where the RE spin relaxation can occur via different channels. First, there is direct coupling of the 4f spins to the lattice due to spin–lattice interaction mediated by their large orbital moments[35–37]—in our model incorporated as α_{Dy}^{ph}. Second, the intraatomic exchange of the Dy 4f moments to its delocalized 5d6sp electron spins provides an indirect coupling to the hot conduction electrons. This opens a relaxation channel in terms of spin pumping, where angular momentum is transferred from the 4f to the 5d6sp orbitals[34,38] and subsequently dissipated via electron-magnon-scattering (α_{Dy}^{el}) analogous to the damping of the Co 3d moments.

The magnitude of the spin-relaxation rates α_i^{ν} is, hereby, highly sensitive to the elemental spin–orbit coupling. In fact, it was found that the damping α_i^{ν} scales quadratically with the spin–orbit coupling parameter[6,7,39] in the high temperature

regime, as used in our fs XMCD experiments. As the atomic-like Dy 4f electrons obey Hund's rules, they exhibit a large orbital moment of $L \approx 5\,\mu_B$ in $DyCo_5$,[11] which leads to strong spin–orbit coupling and, hence, to: 1) large single-ion magnetic anisotropy and to 2) large magnetization damping in the Dy sublattice. This is, for instance, in contrast to the *S*-ion state with $L = 0$ that is found in pure Gd and Gd-based ferrimagnets. In these systems, there is only a weak intrinsic magnetic anisotropy and damping stemming from the Gd 5d moments.[26,37,40,41]

The orbital moments of the 3d electrons of the Co sublattice are almost fully quenched, due to their itinerant character, with residual moments of only ≈ 0.1–$0.2\,\mu_B$.[42,43] This reduces the effective spin–orbit interaction in the TM sublattice significantly compared with the RE ($L \gg 0$) sublattice, and thus, magnetic damping and anisotropy of the TM sublattice are, in general, much weaker. This discrepancy in the elemental spin–orbit coupling strengths ($\lambda_{Dy} = 235$ meV vs $\lambda_{Co} = 70$ meV, see the previous study[44]) in combination with the different origins of magnetic damping in the RE and TM sublattices supports the choice for our spin model and can, therefore, explain the differences in magnetic damping retrieved from our data.

3. Conclusion

To conclude, we have performed an fs laser pump—XMCD probe study of the ultrafast demagnetization and the subsequent remagnetization in a highly anisotropic ferrimagnetic $DyCo_5$ alloy. The transient dynamics of the system is described by an ultrafast and distinct demagnetization of the elemental constituents. ASD simulations using ab initio model parameters can reproduce the experimental results only using largely different values of the magnetic damping parameters for each element, namely, $\alpha_{Co} = 0.004$ and $\alpha_{Dy} = \alpha_{el} + \alpha_{ph} = 0.03$. These combined theoretical and experimental results provide clear evidence for an element-specific magnetization damping in a strongly exchange-coupled magnetic alloy, with far reaching consequences for modeling various ultrafast magnetic phenomena, such as ultrafast demagnetization,[28,29,45] helicity-dependent all-optical switching,[46,47] or thermally induced magnetization reversal.[3,9,48,49] As, microscopically, the damping parameter is connected to the spin–orbit coupling strength, we expect these findings to apply to all compounds with strongly distinct spin–orbit coupling of the constituent elements. Hence, future modeling approaches, which rest on ASD for the treatment of dynamic magnetic phenomena, such as demagnetization, switching, etc., will have to consider this for an accurate description of the transient spin dynamics.

Supporting Information

Supporting Information is available from the Wiley Online Library or from the author.

Acknowledgements

I.R. acknowledges funding from the Federal Ministry of Education and Research (BMBF) through project 05K16BCA (Femto-THz-X) and European Research Council through project TERAMAG (Grant No. 681917). R.A. acknowledges funding from BMBF through project 05K10PC2. U.N. acknowledges financial support from the Deutsche Forschungsgemeinschaft via SFB 1432. A.D. and L.S. are grateful for the support by the Hungarian National Scientific Research Fund (NKFIH) under project Nos. K131938 and PD134579, as well as by the NRDI Fund (TKP2020 IES, Grant No. BME-IE-NAT). The authors thank Christian Schüßler-Langeheine and Niko Pontius for their help with the slicing measurements and Helmholtz-Zentrum Berlin for the allocation of synchrotron radiation beam time.

Open access funding enabled and organized by Projekt DEAL.

Conflict of Interest

The authors declare no conflict of interest.

Data Availability Statement

The data that support the findings of this study are available from the corresponding author upon reasonable request.

Keywords

atomistic spin dynamics simulations, femtosecond X-ray spectroscopy, ferrimagnets, magnetization damping, ultrafast magnetism

Received: January 22, 2021
Revised: March 9, 2021
Published online: May 6, 2021

[1] A. Kirilyuk, A. V. Kimel, T. Rasing, *Rev. Mod. Phys.* **2010**, *82*, 2731.
[2] K. Carva, P. Balaz, I. Radu, *Laser-Induced Ultrafast Magnetic Phenomena*, Vol. *26*, Elsevier, Amsterdam/New York **2017**, pp. 291–463.
[3] I. Radu, K. Vahaplar, C. Stamm, T. Kachel, N. Pontius, H. A. Dürr, T. A. Ostler, J. Barker, R. F. L. Evans, R. W. Chantrell, A. Tsukamoto, A. Itoh, A. Kirilyuk, T. Rasing, A. V. Kimel, *Nature* **2011**, *472*, 205.
[4] S. Wienholdt, D. Hinzke, K. Carva, P. M. Oppeneer, U. Nowak, *Phys. Rev. B* **2013**, *88*, 020406.
[5] N. Kazantseva, U. Nowak, R. W. Chantrell, J. Hohlfeld, A. Rebei, *Europhys. Lett.* **2008**, *81*, 27004.
[6] V. Kamberský, *Czechoslovak J. Phys. B* **1984**, *34*, 1111.
[7] H. Ebert, S. Mankovsky, D. Ködderitzsch, P. J. Kelly, *Phys. Rev. Lett.* **2011**, *107*, 066603.
[8] R. Mondal, M. Berritta, P. M. Oppeneer, *Phys. Rev. B* **2016**, *94*, 144419.
[9] T. A. Ostler, J. Barker, R. F. L. Evans, R. W. Chantrell, U. Atxitia, O. Chubykalo-Fesenko, S. E. Moussaoui, L. L. Guyader, E. Mengotti, L. J. Heyderman, F. Nolting, A. Tsukamoto, A. Itoh, D. Afanasiev, B. A. Ivanov, A. M. Kalashnikova, K. Vahaplar, J. Mentink, A. Kirilyuk, T. Rasing, A. V. Kimel, *Nat. Commun.* **2012**, *3*, 666.
[10] R. Moreno, T. A. Ostler, R. W. Chantrell, O. Chubykalo-Fesenko, *Phys. Rev. B* **2017**, *96*, 014409.
[11] A. Donges, S. Khmelevskyi, A. Deak, R.-M. Abrudan, D. Schmitz, I. Radu, F. Radu, L. Szunyogh, U. Nowak, *Phys. Rev. B* **2017**, *96*, 024412.
[12] A. A. Ünal, S. Valencia, F. Radu, D. Marchenko, K. J. Merazzo, M. Vázquez, J. Sánchez-Barriga, *Phys. Rev. Appl.* **2016**, *5*, 064007.
[13] F. Radu, R. Abrudan, I. Radu, D. Schmitz, H. Zabel, *Nat. Commun.* **2012**, *3*, 715.
[14] T. Seifert, U. Martens, S. Günther, M. A. W. Schoen, F. Radu, X. Z. Chen, I. Lucas, R. Ramos, M. H. Aguirre, P. A. Algarabel,

A. Anadón, H. S. Körner, J. Walowski, C. Back, M. R. Ibarra, L. Morellın, E. Saitoh, M. Wolf, C. Song, K. Uchida, M. Münzenberg, I. Radu, T. Kampfrath, *SPIN* **2017**, *07*, 1740010.
[15] F. Radu, J. Sánchez-Barriga, *Ferrimagnetic Heterostructures for Applications in Magnetic Recording*, Elsevier, Amsterdam/New York **2018**, pp. 267–331.
[16] R. Abrudan, F. Brüssing, R. Salikhov, J. Meermann, I. Radu, H. Ryll, F. Radu, H. Zabel, *Rev. Sci. Instrum.* **2015**, *86*, 063902.
[17] K. Holldack, J. Bahrdt, A. Balzer, U. Bovensiepen, M. Brzhezinskaya, A. Erko, A. Eschenlohr, R. Follath, A. Firsov, W. Frentrup, L. Le Guyader, T. Kachel, P. Kuske, R. Mitzner, R. Müller, N. Pontius, T. Quast, I. Radu, J.-S. Schmidt, C. Schüßler-Langeheine, M. Sperling, C. Stamm, C. Trabant, A. Föhlisch, *J. Synchrotron Radiat.* **2014**, *21*, 1090.
[18] I. A. Abrikosov, H. L. Skriver, *Phys. Rev. B* **1993**, *47*, 16532.
[19] A. Ruban, H. Skriver, *Comput. Mater. Sci.* **1999**, *15*, 119.
[20] A. Liechtenstein, M. Katsnelson, V. Antropov, V. Gubanov, *J. Magn. Magn. Mater.* **1987**, *67*, 65.
[21] H. Ebert, A. Perlov, S. Mankovsky, *Solid State Commun.* **2003**, *127*, 443.
[22] L. Oroszlány, A. Deák, E. Simon, S. Khmelevskyi, L. Szunyogh, *Phys. Rev. Lett.* **2015**, *115*, 096402.
[23] U. Nowak, *Classical Spin Models*, Wiley, New York **2007**.
[24] M. Ellis, T. Ostler, R. Chantrell, *Phys. Rev. B* **2012**, *86*, 174418.
[25] B. Frietsch, J. Bowlan, R. Carley, M. Teichmann, S. Wienholdt, D. Hinzke, U. Nowak, K. Carva, P. M. Oppeneer, M. Weinelt, *Nat. Commun.* **2015**, *6*, 8262.
[26] I. Radu, G. Woltersdorf, M. Kiessling, A. Melnikov, U. Bovensiepen, J.-U. Thiele, C. Back, *Phys. Rev. Lett.* **2009**, *102*, 117201.
[27] I. Radu, C. Stamm, A. Eschenlohr, F. Radu, R. Abrudan, K. Vahaplar, T. Kachel, N. Pontius, R. Mitzner, K. Holldack, A. Föhlisch, T. A. Ostler, J. H. Mentink, R. F. L. Evans, R. W. Chantrell, A. Tsukamoto, A. Itoh, A. Kirilyuk, A. V. Kimel, T. Rasing, *SPIN* **2015**, *5*, 1550004.
[28] N. Bergeard, V. López-Flores, V. Halté, M. Hehn, C. Stamm, N. Pontius, E. Beaurepaire, C. Boeglin, *Nat. Commun.* **2014**, *5*, 3466.
[29] T. Ferté, N. Bergeard, L. Le Guyader, M. Hehn, G. Malinowski, E. Terrier, E. Otero, K. Holldack, N. Pontius, C. Boeglin, *Phys. Rev. B* **2017**, *96*, 134303.
[30] A. B. Schmidt, M. Pickel, M. Donath, P. Buczek, A. Ernst, V. P. Zhukov, P. M. Echenique, L. M. Sandratskii, E. V. Chulkov, M. Weinelt, *Phys. Rev. Lett.* **2010**, *105*, 197401.
[31] K. Carva, M. Battiato, P. M. Oppeneer, *Phys. Rev. Lett.* **2011**, *107*, 207201.
[32] K. Carva, M. Battiato, D. Legut, P. M. Oppeneer, *Phys. Rev. B* **2013**, *87*, 184425.
[33] E. Turgut, D. Zusin, D. Legut, K. Carva, R. Knut, J. M. Shaw, C. Chen, Z. Tao, H. T. Nembach, T. J. Silva, S. Mathias, M. Aeschlimann, P. M. Oppeneer, H. C. Kapteyn, M. M. Murnane, P. Grychtol, *Phys. Rev. B* **2016**, *94*, 220408.
[34] S. Mankovsky, D. Ködderitzsch, G. Woltersdorf, H. Ebert, *Phys. Rev. B* **2013**, *87*, 014430.
[35] A. Eschenlohr, M. Sultan, A. Melnikov, N. Bergeard, J. Wieczorek, T. Kachel, C. Stamm, U. Bovensiepen, *Phys. Rev. B* **2014**, *89*, 214423.
[36] M. Amann, U. Nowak, *J. Magn. Magn. Mater.* **2019**, *469*, 217.
[37] B. Frietsch, A. Donges, R. Carley, M. Teichmann, J. Bowlan, K. Döbrich, K. Carva, D. Legut, P. Oppeneer, U. Nowak, M. Weinelt, *Sci. Adv.* **2020**, *6*, eabb1601.
[38] M. Fähnle, C. Illg, *J. Phys.: Condens. Matter* **2011**, *23*, 493201.
[39] S. Bhagat, P. Lubitz, *Phys. Rev. B* **1974**, *10*, 179.
[40] M. Wietstruk, A. Melnikov, C. Stamm, T. Kachel, N. Pontius, M. Sultan, C. Gahl, M. Weinelt, H. A. Dürr, U. Bovensiepen, *Phys. Rev. Lett.* **2011**, *106*, 127401.
[41] G. Woltersdorf, M. Kiessling, G. Meyer, J.-U. Thiele, C. H. Back, *Phys. Rev. Lett.* **2009**, *102*, 257602.
[42] J. Stöhr, *J. Electron Spectrosc. Relat. Phenom.* **1995**, *75*, 253.
[43] O. Eriksson, B. Johansson, R. C. Albers, A. M. Boring, M. S. S. Brooks, *Phys. Rev. B* **1990**, *42*, 2707.
[44] J. M. D. Coey., *Magnetism and Magnetic Materials*, Cambridge University Press, Cambridge, UK **2010**.
[45] E. Oniciuc, L. Stoleriu, D. Cimpoesu, A. Stancu, *Appl. Phys. Lett.* **2014**, *104* 222404.
[46] S. Mangin, M. Gottwald, C.-H. Lambert, D. Steil, V. Uhlíř, L. Pang, M. Hehn, S. Alebrand, M. Cinchetti, G. Malinowski, Y. Fainman, M. Aeschlimann, E. E. Fullerton, *Nat. Mater.* **2014**, *13*, 286.
[47] C. D. Stanciu, F. Hansteen, A. V. Kimel, A. Kirilyuk, A. Tsukamoto, A. Itoh, T. Rasing, *Phys. Rev. Lett.* **2007**, *99*, 047601.
[48] R. B. Wilson, J. Gorchon, Y. Yang, C.-H. Lambert, S. Salahuddin, J. Bokor, *Phys. Rev. B* **2017**, *95*, 180409.
[49] A. Ceballos, A. Pattabi, A. El-Ghazaly, S. Ruta, C. Simon, R. Evans, T. Ostler, R. Chantrell, E. Kennedy, M. Scott, J. Bokor, F. Hellman, *arXiv:1911.09803v3*, **2020**.